

CoMaLit – II. The scaling relation between mass and Sunyaev-Zel’dovich signal for Planck selected galaxy clusters

Mauro Sereno^{1*}, Stefano Ettori^{2,3}, Lauro Moscardini^{1,2,3}

¹*Dipartimento di Fisica e Astronomia, Università di Bologna, Viale Berti Pichat 6/2, 40127 Bologna, Italia*

²*INAF, Osservatorio Astronomico di Bologna, via Ranzani 1, 40127 Bologna, Italia*

³*INFN, Sezione di Bologna, viale Berti Pichat 6/2, 40127 Bologna, Italia*

6 December 2024

ABSTRACT

We discuss the scaling relation between mass and the integrated Compton parameter of a sample of galaxy clusters from the all-sky *Planck* Sunyaev-Zel’dovich catalogue. Masses were measured with either weak lensing, caustics techniques or assuming hydrostatic equilibrium. According to the calibration sample, the slope of the M_{500} – Y_{500} relation is 1.2–1.6, shallower than self-similar predictions, with an intrinsic scatter of 20 ± 10 per cent. The regression method employed accounts for intrinsic scatter in the mass measurements too. The absolute calibration of the relation is most difficult to ascertain due to systematic differences of $\sim 20 - 40$ per cent in mass estimates reported by separate groups. We find that Planck cluster mass estimates suffer from a mass dependent bias.

Key words: galaxies: clusters: general – galaxies: clusters: intracluster medium – gravitational lensing: weak – galaxies: kinematics and dynamics – methods: statistical

1 INTRODUCTION

Clusters of galaxies are big and interesting (Voit 2005). Understanding of their formation and evolution comes from theory and numerical simulations, which usually characterize clusters by their mass, or from observations at a variety of wave-lengths (Limousin et al. 2013). We can probe their X-ray luminosity and temperature, the optical richness and luminosity, the Sunyaev-Zel’dovich (SZ) flux and the weak lensing (WL) shear and convergence and so on.

A crucial piece of the puzzle is the accurate knowledge of scaling relations between cluster properties. Scaling relations enable us to confront theoretical predictions with actual data and test at once cosmological models (Planck Collaboration et al. 2013c) and cluster physics (Battaglia et al. 2012; Ettori 2013). Mass-observable scaling relations are at the basis of all work that exploits the abundance of galaxy clusters for constraining cosmological parameters (Vikhlinin et al. 2009; Mantz et al. 2010; Rozo et al. 2010).

The mass dependence of cluster observables is strictly connected to the main gravitational processes driving the cluster evolution (Kaiser 1986; Giodini et al. 2013). Departures from these self-similar expectations show imprints of the non gravitational phenomena which occur during the formation and evolution of clusters, such as feedback and non-thermal processes (Maughan et al. 2012; Ettori 2013).

Likewise, the scatter around the scaling relations probes the variety of cluster radial structures and morphologies, the state of

the intracluster gas, the presence or absence of a cool core, and the dynamical state (Arnaud et al. 2010; Rasia et al. 2012).

The ability to robustly measure empirical cluster scaling relations is crucial (Roza et al. 2014b). In this context, the relation between mass and SZ flux has a prominent role. It is expected to have small intrinsic scatter (Kay et al. 2012; Battaglia et al. 2012) and must be accurately calibrated to constrain cosmological parameters using number counts (Planck Collaboration et al. 2013c). As it is usual for scaling relations, it is modelled as a power law,

$$\left[\frac{H(z)}{H_0} \right]^{-2/3} \left[\frac{D^2(z) Y_{500}}{10^{-4} \text{Mpc}^2} \right] = 10^\alpha \left[\frac{M_{500}}{M_{\text{pivot}}} \right]^\beta, \quad (1)$$

where $H(z)$ is the redshift dependent Hubble parameter, $H_0 \equiv H(z=0)$, D is the angular diameter distance to the cluster, M_{500} and Y_{500} denote the mass and the spherically integrated Compton parameter within a sphere of radius r_{500} enclosing a mean overdensity of 500 times the critical density at the cluster redshift and M_{pivot} is a pivotal mass.

Planck’s cluster count cosmology results (Planck Collaboration et al. 2013c) differ from those from the Planck’s measurements of the primary CMB (Cosmic Microwave Background) temperature anisotropies (Planck Collaboration et al. 2013b). Discrepancies might hinge on inaccurate calibration of the scaling relation. The larger values of the amplitude of the matter power spectrum, σ_8 , and the matter density parameter, Ω_M , preferred by CMB experiments might be accommodated by a mass bias of about 45 per cent, where the bias is defined through the ratio of the measured to the ‘true’ mass $M_{500}^{\text{Meas}} = (1 - b) M_{500}^{\text{True}}$ (Planck Collaboration

* E-mail: mauro.serenio@unibo.it (MS)

et al. 2013c). This level of bias is larger than expected. Based on numerical simulations, Planck Collaboration et al. (2013c) adopted a default value of $b = 0.2$, which was assumed as a prior in their analysis. From comparison with a sample of weak lensing masses, von der Linden et al. (2014) found a larger bias, $b = 0.30 \pm 0.06$.

Self-similar models predict a slope of the M_{500} – Y_{500} relation (in logarithmic variables) of $\beta = 5/3$ (Giodini et al. 2013; Ettori 2013). Self-similarity only accounts for gravity processes, which are dominant at the scales of the massive clusters selected by SZ flux. Numerical simulations confirm that the M_{500} – Y_{500} relation has little scatter ($\lesssim 10$ per cent in the local Universe), it is nearly insensitive to the cluster gas physics and it evolves to redshift $\lesssim 1$ in agreement with the self-similar expectation of $\beta \sim 1.6 - 1.8$ (Battaglia et al. 2012; Kay et al. 2012).

This is the second of a series of papers devoted to the COmparison of galaxy cluster MAsses in LITerature (CoMaLit) and to the calibration of scaling relations. In the first paper (Sereno & Ettori 2014, henceforth Paper I), we compared two well regarded mass proxies, the weak lensing (WL) mass and the X-ray determination of the mass based on the hypothesis of hydrostatic equilibrium (HE). We measured the intrinsic scatters, estimated the relative bias and discussed how the intrinsic scatter in the mass proxy affects the scaling relations.

In this second paper, we develop and apply the formalism of Paper I to calibrate the SZ flux estimated by the Planck satellite against mass proxies. We considered masses obtained either from WL analyses (Applegate et al. 2014; Hoekstra et al. 2012; Umetsu et al. 2011), X-ray studies (Donahue et al. 2014; Landry et al. 2013), or the caustic technique (Rines & Diaferio 2006, CS).

The paper is structured as follows. Section 2 reviews some properties of the Planck selected clusters. Section 3 lists the cluster samples used to calibrate the scaling relation. The mass bias affecting Planck masses is discussed in Sec. 4. Section 5 is devoted to highlight some features of the Planck calibration sample. The scaling relation is derived in Sec. 6. Discussion of results and final considerations are contained in Secs. 7, and 8, respectively.

Conventions and notations are as in Paper I. Throughout the paper, we assume a flat Λ CDM cosmology with density parameter $\Omega_M = 0.3$, and Hubble constant $H_0 = 70 \text{ km s}^{-1} \text{ Mpc}^{-1}$; \log is the logarithm to base 10 and \ln is the natural logarithm.

2 SZ SAMPLE

As reference, we considered the clusters from the Planck SZ Catalogue (PSZ, Planck Collaboration et al. 2013a) detected with the Matched Multi-filter method MMF3. This algorithm discovered 883 candidates with detections above signal to noise ratio $S/N = 4.5$ outside the highest-emitting Galactic regions and the Small and Large Magellanic Clouds and outside the point source masks.

A redshift determination is available for 664 among these clusters. The PSZ catalogue spans a broad mass range from 0.1 to $16 \times 10^{14} M_\odot$ at a median redshift of $z \sim 0.22$.

A purer subsample of 189 candidates constructed by selecting the detections above a S/N threshold of 7 outside Galactic and point source masks covering 35 per cent of the sky constitutes the cosmological sample (Planck Collaboration et al. 2013c).

The Planck team determined the M_{500} – Y_{500} relation through multiple steps (Planck Collaboration et al. 2013c). First, the local M_{500}^{HE} – Y_X relation, where Y_X is the X-ray analogue of Y_{500} and it is defined as the product of the gas mass within r_{500} and the spectroscopic temperature outside the core (Kravtsov, Vikhlinin &

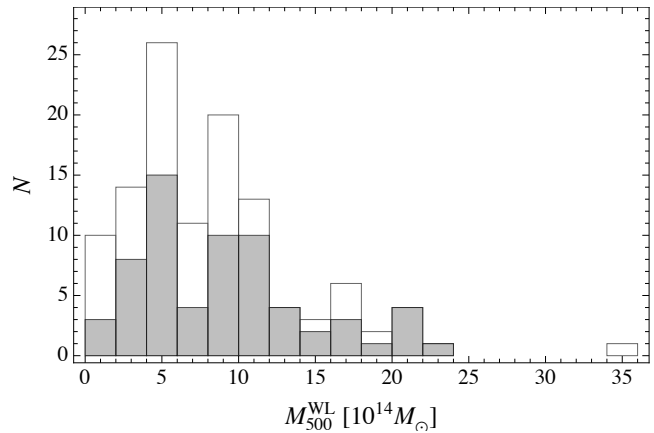


Figure 1. Distribution of the masses M_{500}^{WL} of the clusters in the ‘All’ sample with Planck detections. The white (gray) histogram represents the full (cosmological) sample.

Nagai 2006), was calibrated against the hydrostatic masses M_{500}^{HE} of 20 relatively relaxed local clusters (Arnaud et al. 2010). This local sample is not representative of the SZ selected Planck clusters. Masses estimated through the scaling relation $M_{500}^{\text{HE}} - Y_X$ are denoted $M_{500}^{Y_X}$.

Secondly, the $M_{500}^{Y_X}$ – Y_{500} relation was computed for 71 detections from the Planck cosmological sample for which good quality XMM-Newton observations were available. The SZ signals were re-estimated within a sphere of radius $r_{500}^{Y_X}$, centred on the position of the X-ray peak. Standard redshift evolution was assumed.

For the scaling $M_{500}^{Y_X}$ – Y_{500} , Planck Collaboration et al. (2013c) found $\alpha = -0.186 \pm 0.011$ and $\beta = 1.79 \pm 0.06$ for $M_{\text{pivot}} = 6 \times 10^{14} M_\odot$, see Eq. (1). The Planck team argued that a bias b might still persist in the HE mass measurements, $M_{500}^{\text{HE}} = (1 - b)M_{500}^{\text{True}}$. Based on a suite of different numerical simulations (Battaglia et al. 2012; Kay et al. 2012), they estimated $b = 0.2^{+0.1}_{-0.2}$.

The scaling relation was then used to break the size-flux degeneracy and to estimate cluster masses. In what follows, $M_{500}^{Y_z}$ denotes the mass estimated by the Planck team through the scaling relation $M_{500}^{Y_X}$ – Y_{500} . As reference catalogs for the PSZ clusters, we used the ‘COM_PCCS_SZ-validation_R1.13.fits’ catalog and the additional information in the ‘COM_PCCS_SZ-union_R1.12.fits’ catalog, which are available from the Planck Legacy Archive¹.

3 CALIBRATION SAMPLES

Up to date, there is no statistically complete and copious sample of galaxy clusters with rigorous selection criteria, substantial overlap with the PSZ catalog and direct mass determinations, i.e., mass determinations not relying on scaling relations.

We then considered a number of samples with either WL, CS or HE masses. The main properties of the samples are listed in Table 1. Most of the samples were introduced in Paper I, which we refer to for details and complete references. The overlap between the CLASH and the PSZ samples is quite small. Nevertheless we considered it because it enabled us to perform checks at the very massive end of the cluster distribution.

The list of samples in Table 1 slightly differs from the ensemble

¹ <http://pla.esac.esa.int/pla/aio/planckProducts.html>

Table 1. Calibration samples. Col. 1: name. Col. 2: type of mass measurement (‘WL’ for weak-lensing analyses; ‘CS’ for the caustic technique; ‘HE’ for hydrostatic masses). Col. 3: type of sample (‘F’ for the full sample of PSZ detections; ‘C’ for PSZ clusters in the cosmological subsample). Col. 4: number of clusters in the sample detected by Planck-MMF3. Cols. 5 and 6: typical redshift and dispersion. Cols. 7 and 8: typical mass and dispersion. Col. 9: main reference. Typical values and dispersions are computed as bi-weighted estimators. Masses are in units of $[10^{14} M_{\odot}]$.

Name	Mass	Sample	N_{C1}	z	σ_z	M_{500}	$\sigma_{M_{500}}$	References
All	WL	F	115	0.24	0.14	7.2	5.2	Sereno (2014)
All	WL	C	65	0.22	0.13	8.5	5.7	Sereno (2014)
WTG	WL	F	34	0.35	0.13	11.8	5.2	Applegate et al. (2014)
WTG	WL	C	22	0.31	0.13	12.4	5.6	Applegate et al. (2014)
CLASH-WL	WL	F	11	0.40	0.13	11.0	3.7	Umetsu et al. (2014)
CLASH-WL	WL	C	6	0.37	0.13	13.7	5.4	Umetsu et al. (2014)
CCCP-WL	WL	F	35	0.22	0.07	7.2	3.0	Hoekstra et al. (2012); Mahdavi et al. (2013)
CCCP-WL	WL	C	19	0.21	0.04	8.2	3.2	Hoekstra et al. (2012); Mahdavi et al. (2013)
CIRS	CS	F	22	0.08	0.02	1.9	1.3	Rines & Diaferio (2006)
CIRS	CS	C	10	0.08	0.02	2.9	2.4	Rines & Diaferio (2006)
E10	HE	F	34	0.19	0.07	7.1	3.1	Ettori et al. (2010)
E10	HE	C	27	0.20	0.06	7.3	3.2	Ettori et al. (2010)
CLASH-CXO	HE	F	12	0.39	0.13	10.4	7.6	Donahue et al. (2014)
CLASH-CXO	HE	C	7	0.35	0.13	13.2	6.3	Donahue et al. (2014)
L13	HE	F	29	0.23	0.05	6.1	2.6	Landry et al. (2013)
L13	HE	C	21	0.22	0.05	6.6	2.4	Landry et al. (2013)
CCCP-HE	HE	F	33	0.22	0.08	7.1	3.8	Mahdavi et al. (2013)
CCCP-HE	HE	C	19	0.21	0.04	7.8	3.7	Mahdavi et al. (2013)

of catalogs considered in Paper I. Due to the small number of clusters, we did not consider HE mass determinations in the CLASH sample based on XMM observations. Furthermore, we did not consider the X-ray sample in Bonamente et al. (2012), since their mass determination exploited SZ data from the Sunyaev-Zel’dovich array, which might cause tension with the SZ determination from Planck.

On the other hand, in addition to the samples introduced in Paper I, we also considered a sample of masses estimated with the caustic technique (Rines & Diaferio 2006) and a heterogeneous sample of WL masses as numerous as possible, which we will briefly introduce in the following.

The samples span a large range of masses and redshifts. CLASH and WTG clusters are very massive and at larger redshift. The CIRS clusters, which are quite small and near, lie at the other end of the spectrum.

3.1 Lensing clusters

Sereno (2014) collected from literature data for 405 groups and clusters of galaxies with estimated redshift and WL mass (thereafter, the ‘All’ sample). The redshift range is $0.02 \lesssim z \lesssim 1.5$. Values of M_{500} were either directly taken from the original papers or extrapolated using the quoted density profiles. If necessary, mass estimates were rescaled to the reference cosmological model, see Paper I.

The clusters of this sample were discovered in a variety of ways within X-ray, optical, SZ or WL surveys. The ensemble is very heterogeneous either for the observational facilities, the data analysis, or the selection criteria. As a consequence, the sample is not statistical, which might bias the results. A well-defined selection function can not be implemented and sample inhomogeneity might increase the observed scatter.

On the positive side, the different finding techniques might average out some systematic biases which affect particular subsam-

ples. Biases due to the orientation and internal structure of clusters and the projection effect of large-scale structure are strongly mitigated for a large sample. Since the only criterion for selection is the identification by Planck and because of the variety of finding techniques, we do not expect that the sample suffers from biases plaguing lensing selected samples, such as the over-concentration problem and the orientation bias (Oguri & Blandford 2009; Meneghetti et al. 2011; Sereno & Zitrin 2012).

Very massive clusters at intermediate redshifts are preferential targets for both WL and SZ analyses. 115 WL clusters were identified by Planck too. 65 of them are included in the cosmological sample. The mass distribution is plotted in Fig. 1. Clusters from the cosmological sample do not differentiate themselves from the full sample by mass. According to a Kolmogorov-Smirnov test, there is a 61.5 per cent probability that the masses of the cosmological and full samples are drawn from the same population.

As a matter of fact, WL clusters effectively sample the massive end of the PSZ catalog. This can be verified quantitatively with a Kolmogorov-Smirnov test. For detections with S/N above 7 (10), there is a 5.0 (71.4) per cent probability that the 70 (37) PSZ clusters with WL measurements out of the total 232 (86) clusters follow the total distribution.

The z distributions are compatible at the 14.6 per cent level.

3.2 Cluster Infall Regions in SDSS

The Cluster Infall Regions in SDSS program (CIRS, Rines & Diaferio 2006) studied a sample of 72 nearby clusters from the Data Release 4 of the Sloan Digital Sky Survey (SDSS, Adelman-McCarthy et al. 2006) after selection in X-ray flux and redshift ($z < 0.1$).

Masses were derived from the infall patterns with the caustic technique. We computed M_{500} from the published values of r_{500} and z . Errors were rescaled from mass uncertainties at larger radii.

Only nine clusters from the CIRS sample have a WL mass esti-

Table 2. Mass comparison, $\ln M_{500}^{Y_z} - \ln M_{500}^{WL} = \ln(1 - b^{Y_z})$, for Planck clusters with WL masses. Col. 1: mass catalog used for the calibration. Col. 2: subsample ('F' stands for the full sample of Planck clusters with WL analyses; 'C' refers to the Planck clusters in the cosmological subsample; 'R' refers to the relaxed clusters). Col. 3: number of clusters, N_{C1} . Cols. 4 and 5: central estimate $\mu = \langle \ln(1 - b^{Y_z}) \rangle$ and scatter σ . μ and σ are computed as bi-weighted estimators.

Calibration	Sample	N_{C1}	μ	σ
All	F	115	-0.12 ± 0.05	0.55 ± 0.06
All	F	65	-0.11 ± 0.06	0.50 ± 0.05
WTG	F	34	-0.37 ± 0.07	0.36 ± 0.05
WTG	C	22	-0.37 ± 0.11	0.38 ± 0.06
CLASH-WL	F	11	-0.45 ± 0.10	0.29 ± 0.07
CLASH-WL	C	6	-0.43 ± 0.22	0.34 ± 0.15
CCCP-WL	F	35	0.00 ± 0.06	0.33 ± 0.05
CCCP-WL	C	19	0.10 ± 0.09	0.34 ± 0.09

Table 3. Mass comparison, $\ln M_{500}^{Y_z} - \ln M_{500}^{CS} = \ln(1 - b^{Y_z})$, for Planck clusters with caustic masses. Columns are as in Table 2.

Calibration	Sample	N_{C1}	μ	σ
CIRS	F	22	0.35 ± 0.18	0.79 ± 0.13
CIRS	C	10	0.43 ± 0.30	0.76 ± 0.16

mate. Unfortunately, WL mass determinations for low redshift clusters are usually very noisy. For the CIRS clusters with WL mass, we found a mass ratio $M_{500}^{CS}/M_{500}^{WL}$ with central value 0.90 ± 0.65 and a very large scatter of 1.30.

4 MASS BIAS

The assessment of the bias of Planck masses M^{Y_z} relies on the adopted mass calibration. We computed the bias for different calibration samples following Paper I. We considered the (natural) logarithm of the unweighted mass ratios. Here and in the following, central estimates and the scatters were calculated as bi-weight estimators of the distribution. Uncertainties were estimated with bootstrap resampling with replacement.

Table 4. Mass ratio, $\ln M_{500}^{Y_z} - \ln M_{500}^{HE} = \ln(1 - b^{Y_z})$, for Planck clusters with HE masses. Columns are as in Table 2.

Calibration	SZ sample	N_{C1}	μ	σ
E10	F	34	-0.14 ± 0.08	0.39 ± 0.04
E10	C	27	-0.05 ± 0.09	0.39 ± 0.05
E10	R	10	-0.39 ± 0.07	0.19 ± 0.07
CLASH-CXO	F	12	-0.18 ± 0.16	0.45 ± 0.11
CLASH-CXO	C	7	-0.24 ± 0.21	0.37 ± 0.16
CLASH-CXO	R	3	~ -0.24	
L13	F	29	0.21 ± 0.07	0.34 ± 0.07
L13	C	21	0.20 ± 0.07	0.29 ± 0.06
CCCP-HE	F	33	0.07 ± 0.07	0.43 ± 0.06
CCCP-HE	C	19	0.13 ± 0.13	0.42 ± 0.06
CCCP-HE	R	8	-0.13 ± 0.15	0.38 ± 0.13

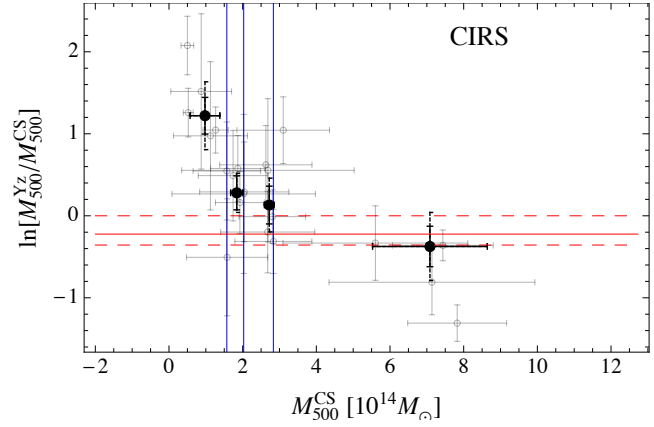


Figure 3. Mass comparison, $\ln(M_{500}^{Y_z}/M_{500}^{CS})$, for Planck clusters in the CIRS sample, as a function of M_{500}^{CS} . Points and lines are as in Fig. 2.

We performed the analysis for the WL samples (see Fig. 2 and Table 2), for the CS sample (see Fig. 3 and Table 3), and for the X-ray samples (see Fig. 4 and Table 4). Whatever the calibration sample, we found that the mass ratio is a decreasing function of the mass proxy, i.e., the bias $b^{Y_z} (\equiv 1 - M^{Y_z}/M^{Pr})$ steadily increases towards large masses. This feature is further highlighted if we group clusters according to the mass proxy. Estimates and trends do not change significantly after restricting the analysis to the cosmological sub-sample.

There are several plausible sources for this trend. Firstly, as discussed in Paper I, the WL, HE and CS masses are scattered proxies of the true mass. Since the intrinsic scatters affecting M^{WL} or M^{CS} and M^{Y_z} are not correlated, for small (large) values of M^{WL} or M^{CS} the estimate of M^{Y_z}/M^{WL} is biased high (low).

The HE mass and M^{Y_z} might be correlated to some degree, being both connected to the pressure profile. However, departures from equilibrium and non-thermal contributions to the pressure, gas clumpiness, the presence of cool cores and the efficiency of feedback processes affect HE masses and the SZ proxy in different ways. These two proxies can then be considered uncorrelated to first approximation.

Secondly, the mass dependent effect might suggest that the scaling relation used to infer M^{Y_z} differs from the one characterizing the calibration sample. As discussed in von der Linden et al. (2014), a wrongly estimated slope β could induce a mass dependent effect.

Thirdly, the Planck clusters are selected in SZ flux and suffer from Malmquist bias. Clusters with strong SZ emission are over-represented, mostly at low masses. The cluster mass obtained from the SZ flux through a scaling relation is then biased high near the flux threshold if no correction for Malmquist bias is applied to the detected flux. Even if the scaling relation used to compute M^{Y_z} was derived after correcting each flux for this bias, the measured values of Y_{500} used to infer the cluster mass through the scaling relation should be corrected too.

Finally, the calibration masses might be systematically biased. We strongly disfavor this last hypothesis since the effect is common for all samples, whose masses were obtained in a number of independent ways.

As for the assessment of the level of bias, this can not be ascertained with confidence due to the hidden systematics affecting mass determinations. As discussed in Paper I, WL mass calibrations are still debated and differences in reported M_{500} from independent

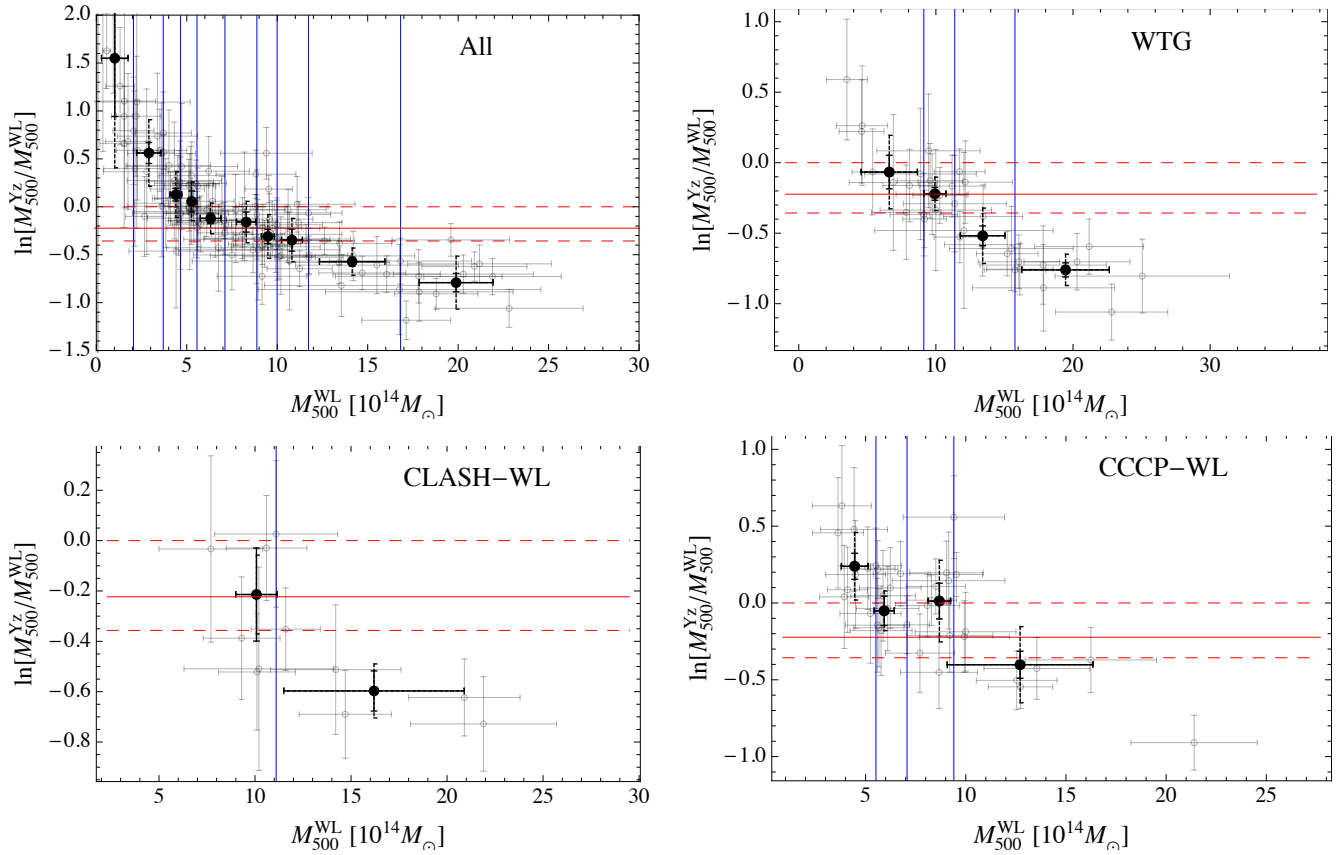


Figure 2. Mass comparison, $\ln(M_{500}^{Y_z}/M_{500}^{WL})$, for Planck clusters with WL masses, as a function of M_{500}^{WL} . Thick black points mark the typical values for groups of clusters binned according to their measured WL mass. Vertical blue lines mark the boundaries of the binning regions. The full error-bars for the binned points denote the $1-\sigma$ uncertainties for the central estimate. The dashed error-bars denote the dispersion. Red lines represent the bias and the relative $1-\sigma$ confidence region estimated by Planck Collaboration et al. (2013c), i.e., $b^{Y_z} = 0.2_{-0.2}^{+0.1}$. The top left, top right, bottom left and bottom right panels show the results for the ‘All’, the WTG, the CLASH-WL, and the CCCP-WL samples, respectively.

analyses can be as large as 40 per cent, well beyond the known level of systematic errors plaguing WL analyses. As a consequence the estimation of the bias ranges from ~ 0 (CCCP-WL) to $\gtrsim 40$ per cent (WTG and CLASH-WL). The bias for the WTG sample is in agreement with the result of von der Linden et al. (2014).

The mass dependent effect shows up in the intrinsic scatter too (see Tables 2, 3 and 4). The dispersion of mass ratios over too large mass intervals is artificially inflated if the assumed slope in the scaling relation for M^{Y_z} is wrong. This would over-estimate the intrinsic scatter measured when we consider the full mass range.

Let us consider the WL samples. Being the scatters uncorrelated, the total measured dispersion should be given by the contributions from the WL measurement errors (~ 15 per cent), the intrinsic scatter in the WL mass, ~ 10 -15 per cent (Rasia et al. 2012; Sereno & Ettori 2014), and the intrinsic scatter in the $M_{500} - Y_{500}$ relation, ~ 15 -20 per cent (Planck Collaboration et al. 2013c). Adding in quadrature we expect the total dispersion to be of the order of ~ 20 -30 per cent, slightly smaller than the measured dispersion (~ 30 -40 per cent).

If we confine the analysis to larger masses, the spread is smaller and the scatter is smaller too, see Fig. 2.

The mass bias found for clusters with caustic masses should behave as for WL clusters (see Fig. 3 and Table 3). Notwithstanding the larger uncertainties, we retrieved the same mass dependence of b_{Y_z} .

Complementing results can be obtained from the comparison of Planck masses to X-ray catalogs. The Planck M^{Y_z} masses should reproduce the HE masses for relaxed clusters. Differently from the WL case, M^{Y_z} is a tracker of the proxy M^{HE} and the bias b^{Y_z} should be null, $M^{Y_z} - M^{\text{HE}} \sim 0$.

Notwithstanding these differences with respect to the WL case, we found that the mass ratio M^{Y_z}/M^{HE} is a decreasing function of the mass proxy M^{HE} (see Fig. 4). This strengthens the hypothesis that there is a mass dependent effect in the calibration of M^{Y_z} .

An alternative hypothesis is that the different dynamical state of the considered X-ray clusters might induce some strong mass-dependent bias in the estimate of the HE mass. We considered subsamples of relaxed clusters for the E10 and the CCCP-HE catalogs (see Fig. 4 and Table 4). We found that the mass-dependence of the bias is still in place whereas the level of bias is increased. However, these subsamples of relaxed clusters are small and we caution against over-interpretation.

5 PLANCK CALIBRATION SAMPLE

The determination of the Planck scaling relation $M_{500}-Y_{500}$ was obtained through a multiple step procedure. The two main pieces are the local $M_{500}^{\text{HE}}-Y_X$ relation and the Y_X-Y_{500} scaling relation.

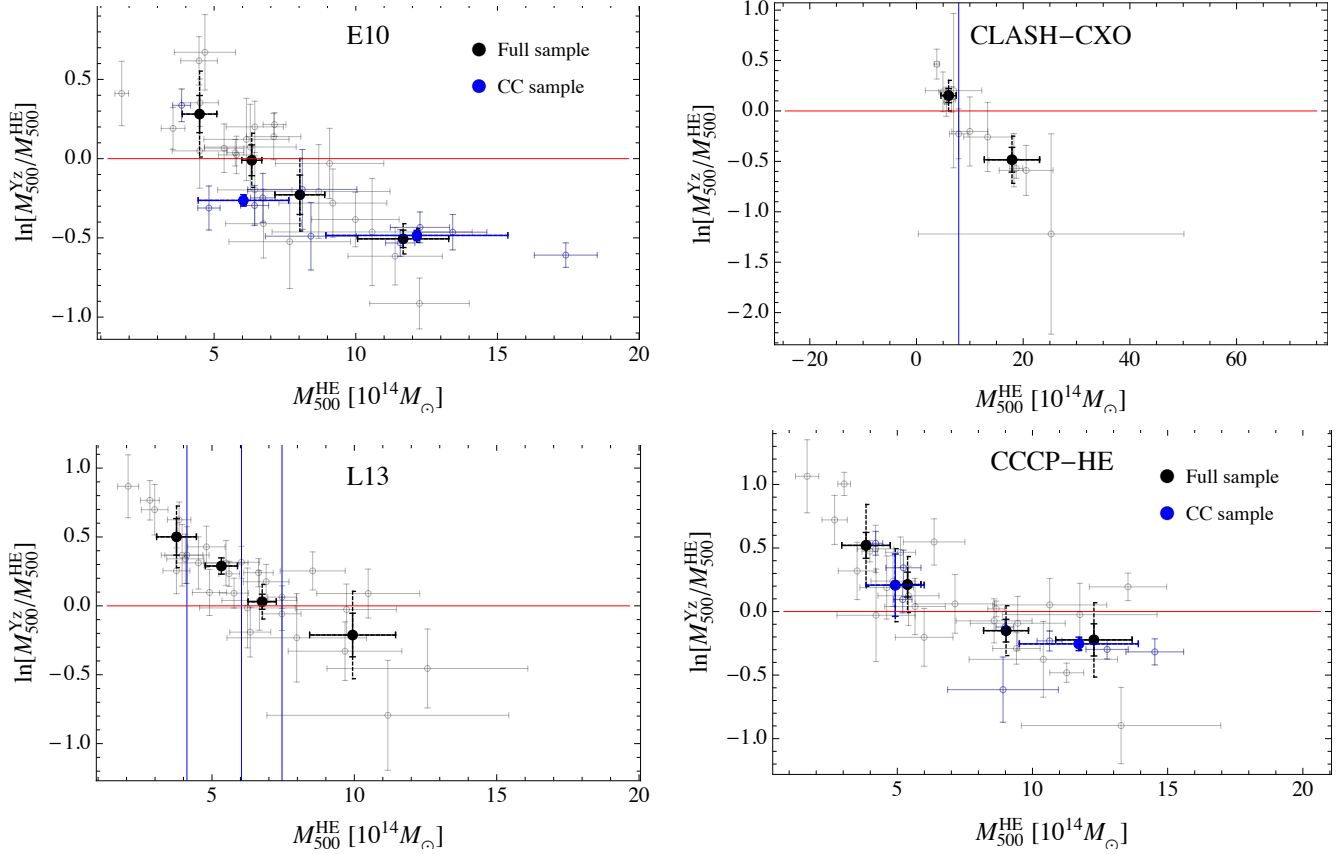


Figure 4. Mass comparison, $\ln(M_{500}^{Yz}/M_{500}^{HE})$, for Planck clusters with HE masses, as a function of M_{500}^{HE} . Black and gray points and blue lines are as in Fig. 2. The red line plots a null bias. Blue points are the analog of the black ones but for the relaxed clusters. The top left, top right, bottom left and bottom right panels show the results for the E10, the CLASH-CXO, the L13, and the CCCP-HE samples, respectively.

Table 5. Mass comparison, $\ln M_{500}^{Yx} - \ln M_{500}^{HE}$, for Planck clusters in the calibration samples. Col. 1: mass catalog used for the calibration. Col. 2: subsample ('C' refers to the Planck clusters in the cosmological subsample; 'R' refers to the relaxed clusters). Col. 3: number of clusters, N_{C1} . Cols. 4 and 5: typical $\ln M_{500}^{Yx}/M_{500}^{HE}$ and scatter. Central estimates and scatters are computed as bi-weighted estimators.

Calibration	Sample	N_{C1}	μ	σ
E10	C	24	-0.08 ± 0.07	0.29 ± 0.05
E10	R	4	~ -0.46	0.04
CLASH-CXO	C	4	-0.27 ± 0.10	0.17 ± 0.07
L13	C	15	0.15 ± 0.05	0.15 ± 0.05
CCCP-HE	C	13	0.04 ± 0.13	0.35 ± 0.09
CCCP-HE	R	5	-0.11 ± 0.08	0.14 ± 0.07

Consequently, the mass calibration based on the Y_X proxy, M^{Yx} , is at the core of the procedure.

By construction the proxy Y_X mimics the SZ flux. The scatter between Y_X and Y_{500} is due to cluster-to-cluster variations in the pressure and density profile (Arnaud et al. 2010), which are known to be not so large. In fact, the slope of the M_{500} – Y_{500} relation determined by the Planck team equals that of the M_{500} – Y_X relation to very good approximation.

Any bias in the estimate of M^{Yz} is then likely connected to

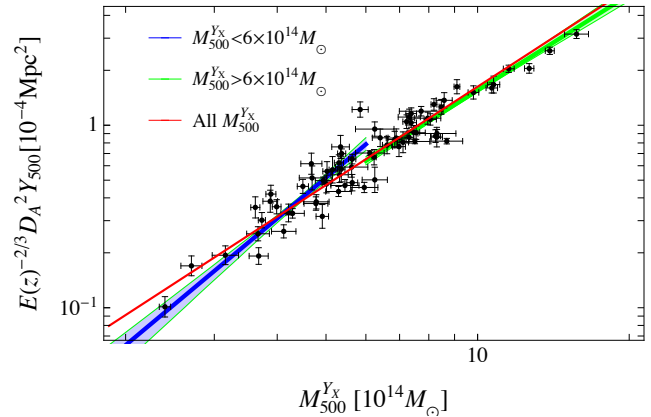


Figure 6. M_{500}^{Yx} versus Y_{500} as measured by the Planck team. SZ fluxes are corrected for Malmquist bias. Regressions in different mass regimes, as obtained with a BCES orthogonal fitting method, are plotted. The blue (green) line considers the clusters with $M_{500}^{Yx} < (>) 6 \times 10^{14} M_{\odot}$. Shaded regions are the $1\text{-}\sigma$ confidence regions. The red line plots the fit for the full mass range.

systematics in the calibration of M^{Yx} . We repeated the comparison of Sec. 4 to look for any bias in the estimate of M^{Yx} of the

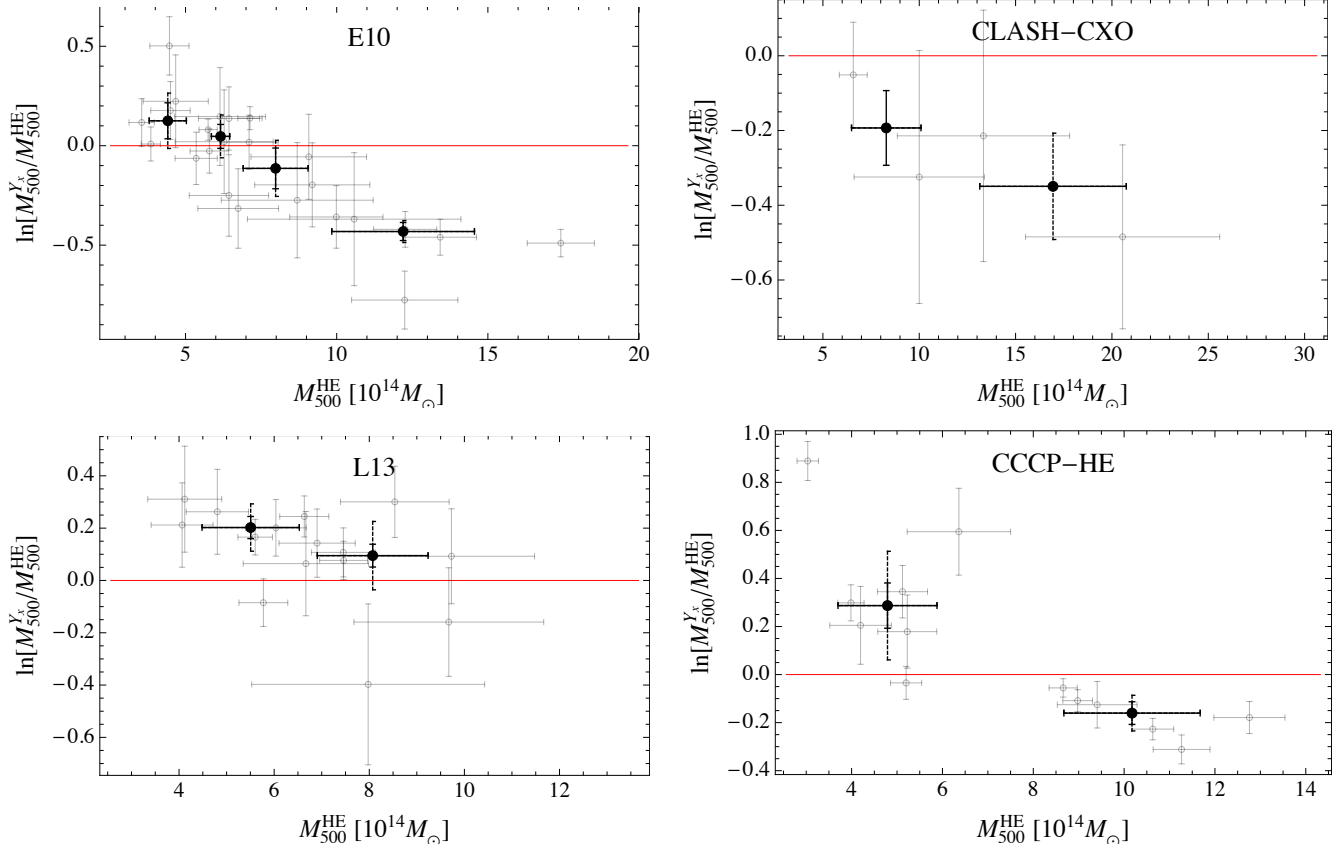


Figure 5. Mass comparison, $\ln(M_{500}^{Yx}/M_{500}^{HE})$, for Planck clusters in the calibration sample with external HE masses, as a function of M_{500}^{HE} . Points and lines are as in Fig. 4. The red line plots a null bias. The top left, top right, bottom left and bottom right panels show the results for the E10, the CLASH-CXO, the L13, and the CCCP-HE samples, respectively.

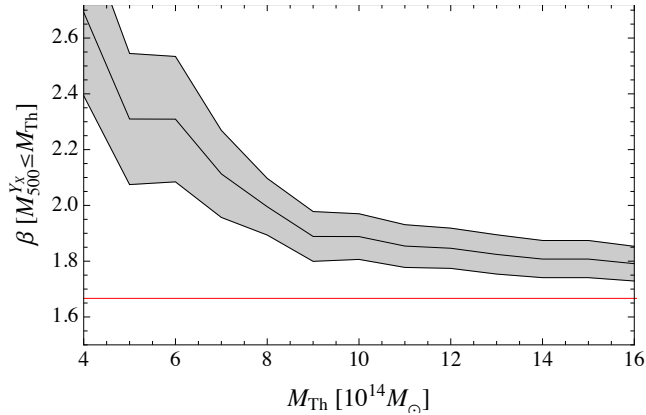


Figure 7. Slope β of the scaling relation $M_{500}^{Yx}-Y_{500}$ as a function of the maximum mass M_{Th} of the considered clusters. We considered the 71 clusters in the Planck calibration sample and performed the linear regression with the BCES orthogonal method after excising clusters whose mass proxy was larger than the threshold, $M_{500}^{Yx} > M_{Th}$. The red line denotes the self-similar slope $\beta = 5/3$.

calibration sample of 71 clusters used to infer the $M_{500}^{Yx}-Y_{500}$ scaling relation.²

² We used data listed in the ‘MY_4_scaling.fits’ catalog, which is publicly available at <http://szcluster-db.ias.u-psud.fr> and reports the masses M_{500}^{Yx} ,

As M_{500}^{Yx} was calibrated to reproduce the HE mass, we limited the analysis to the X-ray calibration samples. Results are summarized in Fig. 5 and Table 5. We retrieved the same trends found for M_{500}^{Yz} (see Sec. 4). Differences between M_{500}^{Yx} and M_{500}^{HE} are mass dependent. The mass ratio $M_{500}^{Yx}/M_{500}^{HE}$ decreases with increasing masses.

As discussed above, the assessment of the level of bias in the normalization is hampered by the systematic differences in the calibration samples (see Table 5). The M_{500}^{Yx} are biased low with respect to the E10 and CLASH-CXO samples, biased high with respect to the L13 sample and consistent with the CCCP-HE sample.

M_{500}^{Yx} should be a good proxy whatever the equilibrium state of the cluster, whereas HE masses are biased low in disturbed systems. There are a few relaxed clusters in common among the various samples, which tentatively suggest that M_{500}^{Yx} might be biased low for relaxed systems.

To further investigate whether the slope in the $M_{500}-Y_{500}$ is biased, we reanalyzed the calibration sample. The Planck team adopted the orthogonal BCES regression method (Akritas & Ber-shady 1996), which we use in this section to simplify comparison and stress the mass dependent effect. SZ fluxes were corrected for Malmquist bias as suggested in Planck Collaboration et al. (2013c). First, we checked that we re-obtained the same regression param-

the SZ Compton parameters, and the cluster-by-cluster Malmquist bias corrections used in Planck Collaboration et al. (2013c).

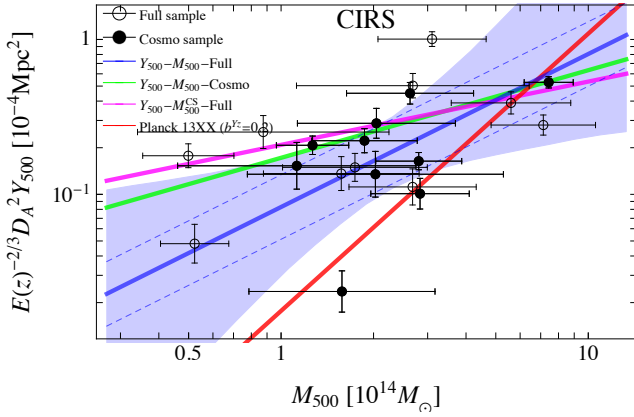


Figure 9. M_{500} versus the spherically integrated Compton parameter for the CIRS sample. The mass proxy is M_{500}^{CS} . Points and lines are as in Fig. 8.

eters when the whole sample of 71 clusters is considered ($\alpha = -0.186 \pm 0.011$ and $\beta = 1.79 \pm 0.06$ for $M_{\text{pivot}} = 6 \times 10^{14} M_{\odot}$).

The value of the slope is strongly impacted by a few clusters with very large mass (see Fig. 6). For the lower mass half of the clusters, $M_{500}^{YX} < 6 \times 10^{14} M_{\odot}$, the slope is $\beta = 2.29 \pm 0.26$; for the more massive half, $M_{500}^{YX} > 6 \times 10^{14} M_{\odot}$, the slope is $\beta = 1.74 \pm 0.11$. The mass dependent effect for different mass thresholds is shown in Fig. 7. The flattening of the slope is driven by the most massive systems. The value of β is approximately self-similar only due to a few very massive clusters with $M_{500}^{YX} \gtrsim 10 \times 10^{14} M_{\odot}$.

We note that the Bayesian method used in the following sections would have preferred a slightly shallower slope for the full sample, $\beta \sim 1.7$. As a matter of fact, among the various BCES methods (Akritas & Bershadsky 1996), the one which is more similar in principle to the regression we performed is the so called BCES($X_2|X_1$), when one tries to predict a quantity given an observed one rather than to find some more intrinsic features of the relation. We checked that the mass dependent effect discussed above does not depend on the specific regression method.

6 SCALING RELATION

In this section we describe how we performed the M_{500} – Y_{500} regression. The value of Y_{500} has to be consistently measured within the over-density radius corresponding to M_{500} . We first estimated the SZ fluxes and then we performed the regression based on the Bayesian technique detailed in Paper I.

6.1 SZ signal

To study the scaling relation between mass and SZ flux, we re-computed the spherically integrated Y_{500} of the PSZ clusters with external WL, CS or HE mass determination within the radius r_{500} . The prior on r_{500} reduces the size-flux degeneracy. As probability distribution, we used

$$p_{\text{PSZ1}}(Y_{500}, r_{500}) \propto \mathcal{L}_{\text{PSZ1}}(Y_{500}, r_{500}) P(r_{500}), \quad (2)$$

where $\mathcal{L}_{\text{PSZ1}}(Y_{500}, r_{500})$ is the likelihood of Y_{500} and r_{500} as obtained by the Planck team with the Matched Multi-Filter method

Three.³ $P(r_{500})$ is the Gaussian prior on r_{500} as determined from the external information on M_{500} (either from WL, X-ray or caustic analyses). We computed the SZ signal as

$$Y_{500} = \int Y'_{500} p_{\text{PSZ1}}(Y'_{500}, r_{500}) dr_{500}. \quad (3)$$

The full uncertainty covariance matrix was derived in a similar way. The posterior marginalized distribution of r_{500} simply follows the prior.

We tested the above procedure against the Y_z reported in the validation catalogue. The main difference between the computation of Y_z reported in the Planck catalog or the values Y_{500} computed as in Eq. (3) consists in the assumed prior. Y_z assumed the Planck M_{500} – Y_{500} scaling relation. We assumed a prior on r_{500} as derived from the mass knowledge.

To compare our estimate of Y_{500} to Y_z , we then assumed as r_{500} the radius derived from the listed M_{500}^{Yz} . For the 663 clusters with known redshift detected with the MMF3 method, we found $Y_{500}/Y_z \sim 1.02 \pm 0.02$. Breaking the size-flux degeneracy through the scaling relation rather than assuming a prior on r_{500} from an external determination is slightly less constraining and produces a slightly larger uncertainty on the estimated Y_{500} . For the 663 clusters, we found $\delta Y_{500}/\delta Y_z \sim 0.91 \pm 0.05$.

Our estimates of Y_{500} were based on the original detections. Nevertheless, the error determined by not re-centering the signal around the identified X-ray/optical counterpart is negligible. Firstly, we compared the original Y_z to $Y_{500, \text{PSX}}$, the signal re-extracted at the X-ray position fixing the size to the X-ray size, as provided in the Planck external validation catalog (Planck Collaboration et al. 2013a). For the 869 clusters with complete information, $Y_{500, \text{PSX}}/Y_z \sim 1.00 \pm 0.01$. The typical difference, $\Delta Y = Y_{\text{PSX}} - Y_z$, is ~ 0.2 times the quoted error on Y_z .

Secondly, we compared our determination of Y_{500} to the re-extracted values obtained by the Planck collaboration for their calibration cosmological sample of 71 clusters. For consistency, as prior for r_{500} we used the estimated r_{500}^{YX} , i.e., the radius corresponding to M_{500}^{YX} . We found $Y_{500}/Y_{500, \text{PSX}} \sim 1.0 \pm 0.1$. The typical deviation, $\Delta Y = Y_{500, \text{PSX}} - Y_{500}$, is ~ -0.1 times the uncertainty on Y_{500} . As for the uncertainty, we found $\delta Y_{500}/\delta Y_{500, \text{PSX}} \sim 1.07 \pm 0.12$.

We can then conclude that our procedure to compute Y_{500} is reliable and that re-extracting and re-centering the signal would not have significantly impacted our results.

6.2 Regression

The regression was implemented through a Bayesian method (Andreon & Hurn 2012). We modelled the M_{500} – Y_{500} relation with a single power law, see Eq. (1). The linear regression was performed in decimal logarithmic variables,

$$\log \tilde{Y}_{500} \pm \delta_{\log \tilde{Y}_{500}} \sim \alpha + \beta \log \tilde{M}_{500} \pm \sigma_Y \quad (4)$$

$$\log M^{\text{Pr}} \pm \delta_{\log M^{\text{Pr}}} \sim \log M_{500} \pm \sigma_X \quad (5)$$

where $\tilde{Y}_{500} \equiv (H(z)/H_0)^{-2/3} (D^2(z) Y_{500}/10^{-4} \text{Mpc}^2)$ and $\tilde{M}_{500} \equiv M_{500}/M_{\text{pivot}}$. The intrinsic scatters σ_Y and σ_X are assumed to be uncorrelated.

Since the SZ flux is computed within r_{500} , Y_{500} and M_{500}

³ We retrieved the likelihood functions from the catalog ‘COM_PCCS_SZ-MMF3_R1.12.fits’, which is publicly available from the Planck Legacy Archive.

Table 6. Parameters of the scaling relation $M_{500}-Y_{500}$ based on WL samples. Col. 1: sample used for mass calibration; col. 2: C or F denotes the cosmological or the full SZ sample, respectively; col. 3: number of clusters in the sample, N_{cl} ; cols. 4, 5: intercept and slope of the scaling relation; col 6: intrinsic scatter of Y_{500} with respect to the fitted scaling relation $Y_{500} - M_{500}$; col 7: intrinsic scatter of the proxy mass, M_{500}^{WL} with respect to the true mass M_{500} . Listed values of the scatters refer to the natural logarithm, $\sigma_{\ln X} = \sigma_X \ln(10)$. Values in square brackets were fixed in the regression procedure. Quoted values are bi-weight estimators of the posterior probability distribution.

Mass calibration	Sample	N_{cl}	α	β	$\sigma_{\ln Y}$	$\sigma_{\ln X}$
All	F	115	-0.27 ± 0.04	1.22 ± 0.24	0.28 ± 0.13	0.26 ± 0.10
All	F	115	-0.25 ± 0.03	0.95 ± 0.10	0.42 ± 0.04	[0]
All	C	65	-0.30 ± 0.06	1.40 ± 0.31	0.27 ± 0.12	0.21 ± 0.09
All	C	65	-0.25 ± 0.04	1.09 ± 0.17	0.40 ± 0.06	[0]
WTG	F	34	-0.28 ± 0.09	1.13 ± 0.27	0.16 ± 0.07	0.14 ± 0.06
WTG	F	34	-0.24 ± 0.07	1.00 ± 0.21	0.20 ± 0.06	[0]
WTG	C	22	-0.32 ± 0.17	1.25 ± 0.49	0.21 ± 0.10	0.17 ± 0.08
WTG	C	22	-0.24 ± 0.12	0.99 ± 0.33	0.27 ± 0.08	[0]
CLASH-WL	F	11	-0.33 ± 0.33	1.32 ± 0.97	0.27 ± 0.16	0.16 ± 0.09
CLASH-WL	F	11	-0.30 ± 0.25	1.19 ± 0.70	0.28 ± 0.14	[0]
CLASH-WL	C	6	0.09 ± 0.42	0.33 ± 1.06	0.25 ± 0.13	0.23 ± 0.14
CLASH-WL	C	6	0.08 ± 0.29	0.37 ± 0.69	0.27 ± 0.12	[0]
CCCP-WL	F	35	-0.22 ± 0.06	1.56 ± 0.41	0.24 ± 0.12	0.17 ± 0.07
CCCP-WL	F	35	-0.19 ± 0.05	1.23 ± 0.25	0.35 ± 0.07	[0]
CCCP-WL	C	19	-0.14 ± 0.08	1.28 ± 0.52	0.20 ± 0.10	0.15 ± 0.07
CCCP-WL	C	19	-0.10 ± 0.06	1.01 ± 0.36	0.26 ± 0.08	[0]

Table 7. Parameters of the scaling relation $M_{500} - Y_{500}$ based on the CIRS sample. The proxy mass is M_{500}^{CS} . Columns are as in Table 6.

Mass calibration	Sample	N_{cl}	α	β	$\sigma_{\ln Y}$	$\sigma_{\ln X}$
CIRS	F	22	-0.30 ± 0.45	1.01 ± 0.97	0.77 ± 0.34	0.46 ± 0.25
CIRS	F	22	-0.46 ± 0.20	0.68 ± 0.38	0.87 ± 0.20	[0]
CIRS	C	10	-0.32 ± 0.30	0.58 ± 1.07	0.48 ± 0.22	0.44 ± 0.25
CIRS	C	10	-0.36 ± 0.14	0.41 ± 0.43	0.55 ± 0.16	[0]

Table 8. Parameters of the scaling relation $M_{500} - Y_{500}$ based on X-ray samples. The proxy mass is the HE mass. Columns are as in Table 6.

Mass calibration	Sample	N_{cl}	α	β	$\sigma_{\ln Y}$	$\sigma_{\ln X}$
E10	F	34	-0.22 ± 0.04	1.16 ± 0.34	0.24 ± 0.11	0.22 ± 0.09
E10	F	34	-0.20 ± 0.03	0.84 ± 0.17	0.34 ± 0.06	[0]
E10	C	27	-0.18 ± 0.05	0.99 ± 0.42	0.23 ± 0.10	0.23 ± 0.10
E10	C	27	-0.15 ± 0.03	0.65 ± 0.18	0.30 ± 0.05	[0]
CLASH-CXO	F	12	-0.11 ± 0.06	0.89 ± 0.17	0.12 ± 0.06	0.13 ± 0.07
CLASH-CXO	F	12	-0.10 ± 0.04	0.85 ± 0.13	0.11 ± 0.06	[0]
CLASH-CXO	C	7	-0.08 ± 0.08	0.84 ± 0.20	0.13 ± 0.07	0.14 ± 0.09
CLASH-CXO	C	7	-0.08 ± 0.06	0.82 ± 0.15	0.12 ± 0.06	[0]
L13	F	29	-0.09 ± 0.03	1.44 ± 0.27	0.17 ± 0.08	0.13 ± 0.05
L13	F	29	-0.09 ± 0.03	1.28 ± 0.22	0.23 ± 0.06	[0]
L13	C	21	-0.10 ± 0.04	1.63 ± 0.37	0.18 ± 0.09	0.12 ± 0.05
L13	C	21	-0.10 ± 0.03	1.45 ± 0.29	0.24 ± 0.08	[0]
CCCP-HE	F	33	-0.10 ± 0.04	1.15 ± 0.36	0.28 ± 0.13	0.25 ± 0.11
CCCP-HE	F	33	-0.09 ± 0.04	0.83 ± 0.17	0.39 ± 0.07	[0]
CCCP-HE	C	19	-0.04 ± 0.04	0.86 ± 0.27	0.21 ± 0.09	0.24 ± 0.11
CCCP-HE	C	19	-0.03 ± 0.03	0.66 ± 0.15	0.28 ± 0.06	[0]

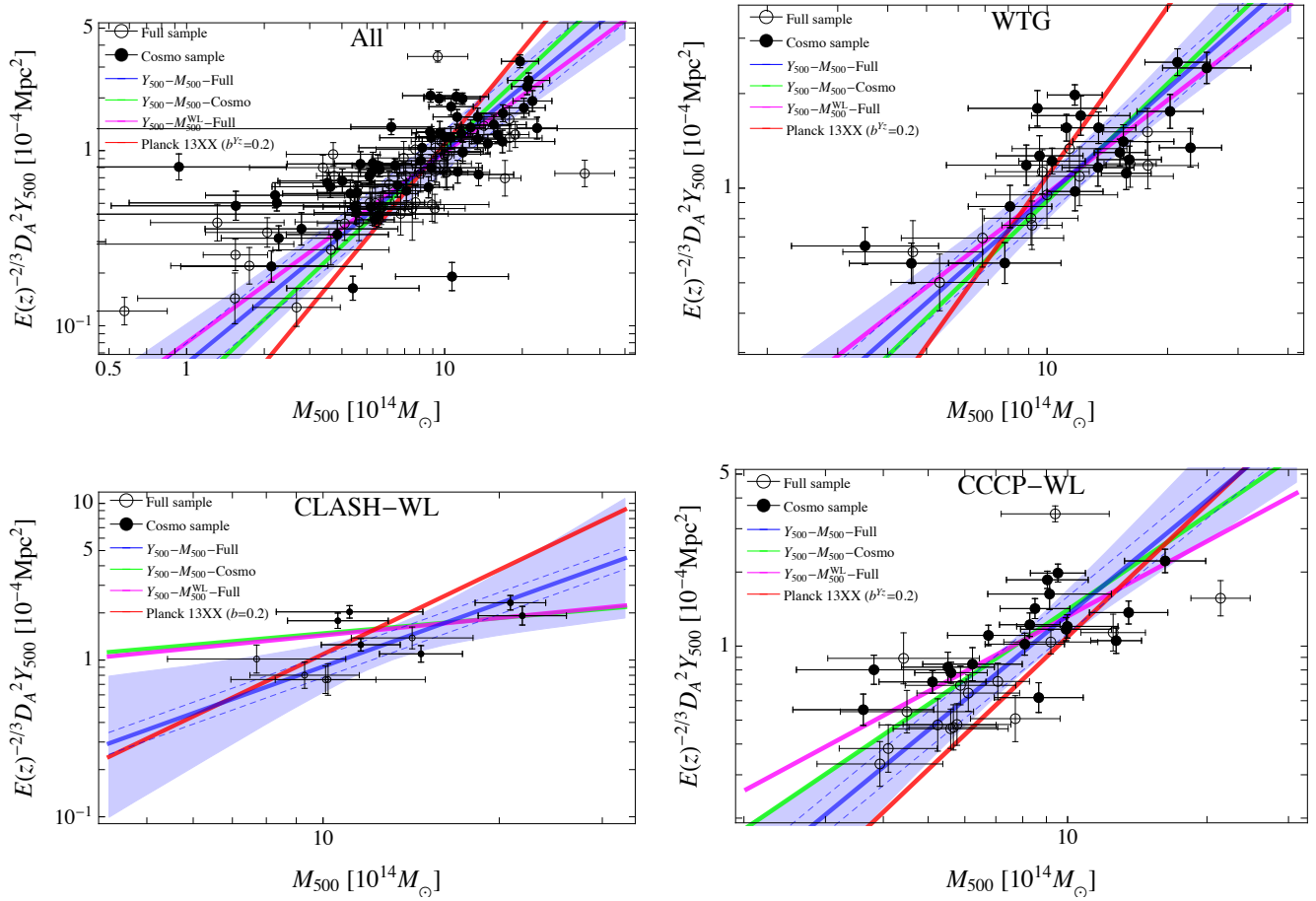


Figure 8. M_{500} versus the spherically integrated Compton parameter for the WL samples. Filled points denote clusters in the cosmological sample; empty circles denote points in the full sample not included in the cosmological sample. The solid blue (green) line marks the mean fitted regression line M_{500} - Y_{500} for the full (cosmological) sample, while the dashed blue lines show this mean plus or minus the intrinsic scatter σ_Y . The shaded blue region encloses the 1- σ confidence region. The magenta line plots the fitted regression line M_{500}^{WL} - Y_{500} for the full SZ sample. The full red line plots the relation determined in Planck Collaboration et al. (2013c) with bias $b^{Y_z} = 0.2$. The top left, top right, bottom left and bottom right panels represent the scaling relations calibrated with the ‘All’, the WTG, the CLASH-WL, and the CCCP-WL samples, respectively.

are correlated. As a result, the errors $\delta_{\log \tilde{Y}_{500}}$ and $\delta_{\log M_{500}^{\text{Pr}}}$ have a joint bivariate distribution with zero mean and covariance matrix as computed in Sec. 6.1.

The true and the observed flux differ for the observational uncertainty $\delta_{\log \tilde{Y}_{500}}$. To account for selection effects, the distribution of the observed flux given a true value was truncated. The Malmquist bias, where bright objects near the flux limit are preferentially detected, was modelled with a step function in the observed SZ flux (Vikhlinin et al. 2009). The threshold was $S/N > 4.5$ (7) for the full (cosmological) sample.

The intrinsic distribution of the independent variable $\log M_{500}$ was approximated with a Gaussian function \mathcal{N} of mean μ and standard deviation τ ,

$$\log M_{500} \sim \mathcal{N}(\mu, \tau). \quad (6)$$

This model fits well the observed distributions (see Fig. 1), and it is suitable for flux selected samples of massive clusters (Andreon & Bergé 2012; Sereno & Ettori 2014). We checked that the impact of modelling the intrinsic distribution with a mixture of Gaussian is minimal and we preferred the simpler hypothesis.

We chose priors as less informative as possible. We adopted uniform priors for the intercept α , and the mean μ . For the vari-

ances, σ^2 and τ^2 , we considered inverse Gamma distributions (Andreon & Hurn 2010). For the slope β , we assumed a Student’s t distribution, which is equivalent to a uniform prior on the direction angle $\arctan \beta$.

Some of the above priors differ from the usual hidden priors adopted in linear fitting procedure. The prior that the slope (instead of the direction angle) is uniformly distributed biases the estimate of β high. At the same time, neglecting positive correlation between measured quantities can as well bias β high. On the other hand, assuming that the true masses are uniformly distributed biases the slope down.

To ease the comparison, we kept the pivot mass fixed to $M_{\text{pivot}} = 6 \times 10^{14} M_{\odot}$ for all cases.

For the numerical implementation of the above statistical scheme, we used the software JAGS⁴, which has been already applied in astronomical contexts (Andreon & Hurn 2012). This approach accounts for heteroscedastic and correlated measurement errors and intrinsic scatter. The parameter space is explored with Gibbs sampling. We verified that an alternative statistical approach

⁴ <http://mcmc-jags.sourceforge.net/>

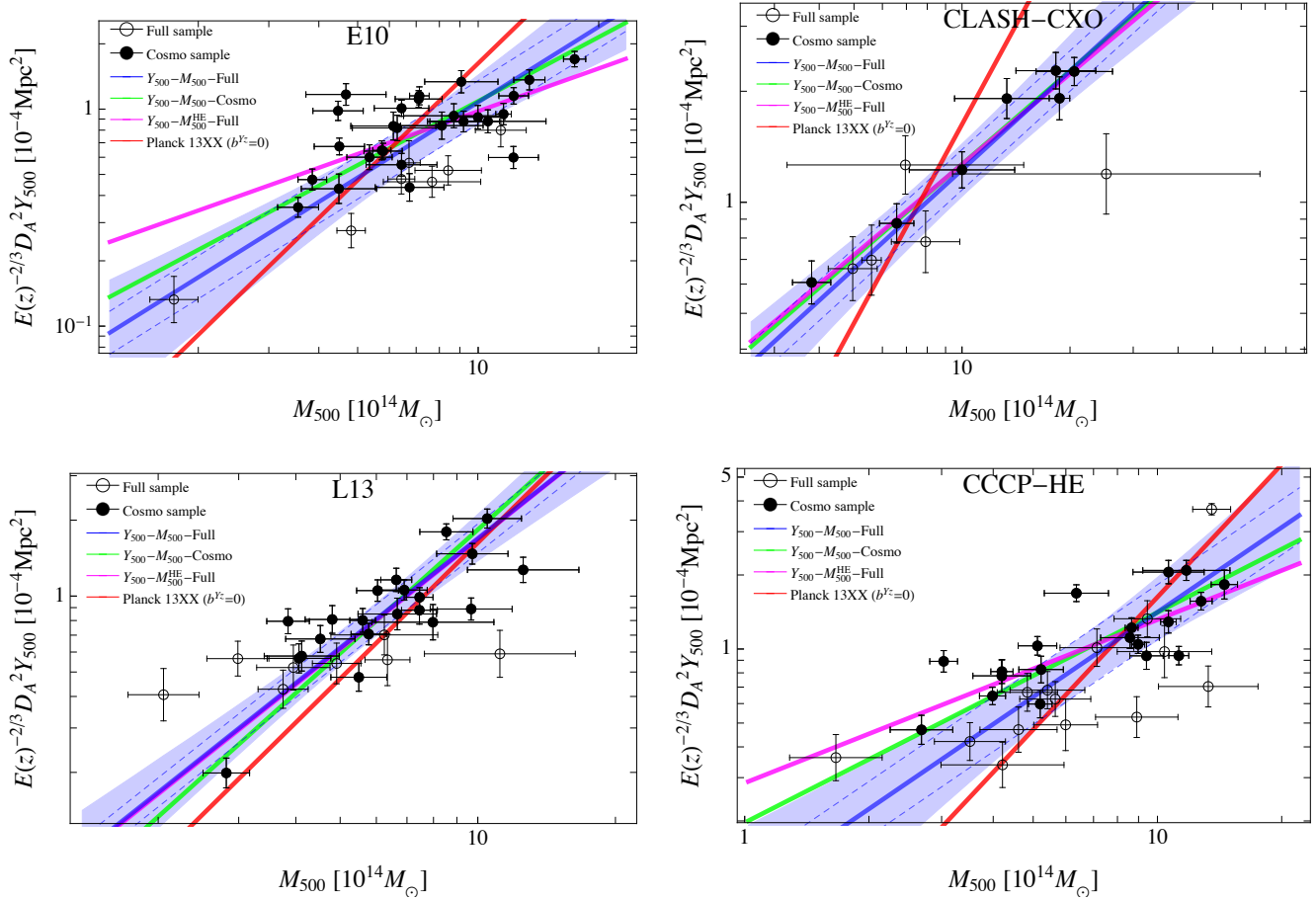


Figure 10. M_{500} versus the spherically integrated Compton parameter for the X-ray samples. The mass proxy is the HE mass. Points and lines are as in Fig. 8. The bias for the scaling in Planck Collaboration et al. (2013c) was fixed to $b^{Y_z} = 0$. The top left, top right, bottom left and bottom right panels represent the scaling relations calibrated with the E10, the CLASH-CXO, the L13 and the CCCP-HE samples, respectively.

based on a likelihood function (Kelly 2007) gives results in full agreement with JAGS, but we preferred JAGS for its faster and stabler convergence.

Regression results for the calibration sample based on WL masses are listed in Table 6 and plotted in Figure 8. Results are consistent among the different samples. The best estimates of the slope ranges from 1.2 to 1.6. These β values are usually slightly shallower, but consistent within the errors, than the self-similar slope of 5/3 and the fitting results of Planck Collaboration et al. (2013c, table A.1) that lie around $\sim 1.6-1.8$ (1.79 ± 0.06 for the Cosmo sample). The shallower slope contributes to the mass dependent bias discussed in Section 4.

Results for the cosmological subsample of clusters are in agreement with the full one.

The intrinsic scatter $\sigma_{\ln Y}$ is of order of 15–30 per cent, in agreement with the estimate in Planck Collaboration et al. (2013c, $\sigma_{\ln Y} \sim 0.15$). As expected, we found a larger scatter in the ‘All’ sample, which we attribute to heterogeneity.

The estimated intrinsic scatter on the WL mass is of order of 15–20 per cent, as expected from numerical simulations and as measured in Paper I.

If we neglect the scatter in the mass proxy, i.e., we fix $\sigma_X = 0$, what we really measure is the scaling of the SZ signal versus the WL mass. As a general trend, the scaling $M_{500}^{\text{WL}}-Y_{500}$ is shallower than $M_{500}^{\text{True}}-Y_{500}$. This is mainly due to clusters with large mass.

Intrinsic scatter as well as observational uncertainties broaden the distribution. In a typical survey, clusters are observed to the same deepness and with similar exposure times and observational facilities. The noise is then nearly uniform with no regard to the clusters mass and the relative uncertainty is smaller for more massive clusters, i.e., clusters with the larger signal to noise ratio. At the low mass tail of the selected cluster mass function, the distribution is then mostly broadened by measurement errors (Eddington bias), whereas at large masses the intrinsic scatter plays a larger role.

The second main difference between the scalings is that the intrinsic scatter σ_Y in the conditional probability $p(Y_{500}|M_{500}^{\text{WL}})$ is larger than in $p(Y_{500}|M_{500}^{\text{True}})$. The SZ flux is a better proxy of the true mass rather than the HE mass and this translates in an inflated scatter in the scaling $M_{500}^{\text{WL}}-Y_{500}$.

Regression results for the CIRS sample (see Table 6 and Figure 8), have too large uncertainties to draw firm conclusions.

The scaling relations derived from the samples with HE masses are similar to the WL case, see Table 6 and Figure 8. The typical values of the slopes are in the range $0.9 \lesssim \beta \lesssim 1.6$, slightly smaller or matching the self-similar value. The intrinsic scatter in the HE mass is estimated to be $0.15 \lesssim \sigma_{\ln X} \lesssim 0.25$. Differently from numerical predictions and as found in Paper I, the scatter in HE masses is slightly larger than in WL masses. The scatter in the SZ flux is of order of $\sim 10-30$ per cent. Analogously to the WL case, we found that the $M_{500}^{\text{HE}}-Y_{500}$ is shallower than $M_{500}^{\text{True}}-Y_{500}$.

Regardless of the calibration sample, we found results that are qualitatively and quantitatively in agreement. The CS case is not constraining, whereas derived scalings based on either WL or HE masses are fully consistent. On the other hand, the level of bias, i.e., the measured intercept α , strongly depends on the assumed sample.

7 DISCUSSION

We review the effects of a flatter slope and how our results compare to previous works and theoretical expectations.

7.1 Other works

Previous works on the scaling relation between mass and integrated Compton parameter are discordant to some degree. Fair comparison is further complicated since slopes determined in different studies might actually refer to different statistical quantities. As a classical example, the slope found with an orthogonal BCES regression is supposed to differ from the BCES slope of the conditional regression (Akritas & Bershady 1996).

Marrone et al. (2012) considered 18 galaxy clusters at $z \sim 0.2$ from the LoCuSS sample (Local Cluster Substructure Survey, Okabe et al. 2010) observed with the Sunyaev-Zel'dovich Array. They found $\beta = 2.3 \pm 0.6$ with a 20 per cent intrinsic scatter. Planck Collaboration et al. (2013d) considered 19 clusters mainly from the LoCuSS sample and found $\beta = 1.7 \pm 0.4$. However, it was later understood that LoCuSS WL masses are biased low due to contamination effects and systematics in shape measurements (Okabe et al. 2013). The underestimate of M_{500} is of the order of 20 per cent (Okabe et al. 2013) and might be mass dependent.

Rozo et al. (2014a) proposed a self-consistent method to derive scaling relations satisfying optical data from SDSS, X-ray data from ROSAT and Chandra, and SZ data from Planck. They derived a slope for the M_{500} - Y_{500} relation of 1.71 ± 0.08 . The bias in the Planck masses can be estimated by equalling the scaling relation in Planck Collaboration et al. (2013c) to the relation in Rozo et al. (2014a). If we require that the predicted SZ fluxes are consistent at $M_{500} = 6 \times 10^{14} M_{\odot}$, we get $b \sim 0.26$.

Our results show some similarities with some other recent studies. Gruen et al. (2014), which performed WL analyses of 5 Planck clusters, found significant discrepancies between the weak lensing masses and the PSZ masses and a shallow slope, $\beta = 0.76 \pm 0.20$. They suggested that a size or redshift dependent bias could affect the analysis of the Planck clusters.

Comparing the Planck masses to the WL masses of the WTG clusters, von der Linden et al. (2014) found evidence for a mass dependence of the calibration ratio. They argued that the origin might hinge on systematic uncertainties in the temperature calibration of the X-ray measurements used to calibrate the Planck cluster masses.

7.2 Theoretical predictions

Self-similar scaling relations aim at describing the intrinsic nature of a complete population of galaxy clusters. We found that the slope of the M_{500} - Y_{500} relation is shallower even if still compatible with the self-similar prediction. In our approach, the slope of the scaling describes the relation between a given mass and the expected values of the SZ flux. An important statistical caveat then applies in the comparison with our result. We were interested in predicting the flux for a given mass, which is a statistically different problem

with respect to trying to find the ‘true’ slope which better describes a population (Akritas & Bershady 1996). Even if the clusters are really self-similar, we expect to recover the self-similar slope only if the covariate is a non-random predictor variable (Andreon & Hurn 2012). This is not the case for cluster masses which are random variable themselves.

The Planck cluster candidates were identified with some criteria that might separate the selected clusters from the undifferentiated population which self-similar models are based on. The very massive clusters in the Planck catalogue might be peculiar objects. Planck detected clusters are characterized by their global properties but we know little about their dynamical status. Irregular morphologies or ongoing merging events might impact the estimate of the cluster mass and the SZ flux to a different degree. In principle, WL estimates can give unbiased estimates even in complex systems, whereas clumpiness and irregularities play a bigger role in the intra-cluster medium distribution (Roncarelli et al. 2013).

The roles of projection effects and orientation in a SZ selected sample should be better understood too. Clusters elongated towards the observer are more luminous and preferentially included in flux-limited samples. A basic spherical analysis over-estimates the lensing mass and the concentration of clusters elongated along the line of sight (Sereno & Umetsu 2011; Giocoli et al. 2013). The distribution of the intra-cluster medium is usually more spherical than the total matter so that triaxiality and orientation have a smaller impact in the estimate of the spherically integrated SZ flux (Sereno et al. 2013). As a consequence, clusters elongated along the line of sight would make the scaling relation shallower at large WL mass. The above effect might induce a mass dependent intrinsic scatter on the WL or HE mass determination.

7.3 Number counts

The slope and the normalization of the scaling relation between M_{500} and Y_{500} strongly impact the expected number of observable clusters above a flux threshold. The Planck team argued that a large mass bias of the order of $b^{Y_z} \sim 40$ per cent might reconcile their cosmological results from number counts with the analysis of the CMB (Planck Collaboration et al. 2013c). This level of bias is in agreement with the mass calibrations based on the WTG and CLASH lensing samples, which implied $b^{Y_z} \sim 30$ –50 percent. On the other hand, the analysis of the CCCP-WL sample does not show such large bias.

The slope of the relation also impacts the number counts. A flatter scaling relation would determine a higher mass threshold for detection. Since massive clusters are rarer, the expected number count of massive clusters above a given flux threshold based on a flatter relation is then smaller than the prediction based on a steeper scaling. The flatter the relation, the larger the value of σ_8 required to match an observed number count. A steeper scaling might then bias low the measured amplitude of the power spectrum.

The above considerations reverse at low masses, where the flatter relation is above the steeper one in the M_{500} - Y_{500} plane. At low masses, a steeper scaling biases high the estimated value of σ_8 .

The effects of the slope at either low or large masses counter-balance each other to some degree. Furthermore, due to selection effects the mass of detectable clusters increases with redshift. A more quantitative assessment on the impact on the total number counts would require the knowledge of the completeness function of the Planck detections.

8 CONCLUSIONS

The effective use of scaling relations hinges on our ability to accurately measure cluster masses. WL and HE masses are accurate but scattered proxies. Numerical simulations have tried to ascertain the level of systematics affecting mass determinations (Rasia et al. 2012; Nelson et al. 2014). The bias in WL masses is mostly connected to irregular morphology and projection effects of the dark matter distribution (Meneghetti et al. 2010; Becker & Kravtsov 2011). The level of such bias is of order of 5-10 per cent with a large scatter (10-25 per cent) (Rasia et al. 2012; Sereno & Ettori 2014). These are known effects which might be reduced with an optimal target selection.

Hydrostatic masses suffer from non-thermal sources of pressure in the intra-cluster medium and temperature inhomogeneity. The X-ray masses are biased low by a large amount of 25-35 per cent with a sizable scatter (see Paper I). X-ray properties of galaxy clusters reported by competing groups reach discrepancies of 50 per cent in mass estimates (Rozo et al. 2014c; Sereno & Ettori 2014).

Issues in instrumental calibration and methodological discrepancies in the data analysis may induce significant errors in the mass determination. Systematics differences in either WL or HE cluster mass impede a definite assessment of the mass bias and a robust calibration of the scaling relations. A consistent analysis of multi-wavelength observables from radio to optical to X-ray bands might help to single out the source of disagreement and to establish unbiased relations (Sereno et al. 2013; Rozo et al. 2014a).

Even though WL masses seem to be more accurate than X-ray estimates, the level of systematic uncertainty is still too high to accurately calibrate scaling relations. Notwithstanding the absolute normalization, we found trends between mass and SZ flux in notable agreement. The further step is an improved characterization of the selection function of the sample and the accurate calibration of the mass estimates.

The redshift evolution of scaling relation was not addressed in this paper. We adopted a self-similar evolution between mass and SZ flux (Giodini et al. 2013). Due to selection limits, clusters at larger redshifts are on average more massive. The bias trend might then be due to a redshift rather than a mass effect (Gruen et al. 2014; von der Linden et al. 2014). The study of the evolution requires a very accurate knowledge of the cluster mass function and the selection function (Andreon & Congdon 2014). Ignoring them can lead to biases larger than the quoted errors.

ACKNOWLEDGEMENTS

MS thanks Stefano Andreon for highlighting discussions. LM and MS acknowledge financial contributions from contracts ASI/INAF I/023/12/0, by the PRIN MIUR 2010-2011 ‘The dark Universe and the cosmic evolution of baryons: from current surveys to Euclid’ and by the PRIN INAF 2012 ‘The Universe in the box: multiscale simulations of cosmic structure’.

REFERENCES

Adelman-McCarthy J. K. et al., 2006, *ApJS*, 162, 38
 Akritas M. G., Bershadsky M. A., 1996, *ApJ*, 470, 706
 Andreon S., Bergé J., 2012, *A&A*, 547, A117
 Andreon S., Congdon P., 2014, *ArXiv*: 1406.1651
 Andreon S., Hurn M. A., 2010, *MNRAS*, 404, 1922

Andreon S., Hurn M. A., 2012, *ArXiv*: 1210.6232
 Applegate D. E. et al., 2014, *MNRAS*, 439, 48
 Arnaud M., Pratt G. W., Piffaretti R., Böhringer H., Croston J. H., Pointecouteau E., 2010, *A&A*, 517, A92
 Battaglia N., Bond J. R., Pfrommer C., Sievers J. L., 2012, *ApJ*, 758, 74
 Becker M. R., Kravtsov A. V., 2011, *ApJ*, 740, 25
 Bonamente M. et al., 2012, *New Journal of Physics*, 14, 025010
 Donahue M. et al., 2014, *ArXiv*: 1405.7876
 Ettori S., 2013, *MNRAS*, 435, 1265
 Ettori S., Gastaldello F., Leccardi A., Molendi S., Rossetti M., Buote D., Meneghetti M., 2010, *A&A*, 524, A68
 Giocoli C., Meneghetti M., Metcalf R. B., Ettori S., Moscardini L., 2013, *ArXiv*: 1311.1205
 Giodini S., Lovisari L., Pointecouteau E., Ettori S., Reiprich T. H., Hoekstra H., 2013, *Space Science Reviews*, 177, 247
 Gruen D. et al., 2014, *MNRAS*, 442, 1507
 Hoekstra H., Mahdavi A., Babul A., Bildfell C., 2012, *MNRAS*, 427, 1298
 Kaiser N., 1986, *MNRAS*, 222, 323
 Kay S. T., Peel M. W., Short C. J., Thomas P. A., Young O. E., Battye R. A., Liddle A. R., Pearce F. R., 2012, *MNRAS*, 422, 1999
 Kelly B. C., 2007, *ApJ*, 665, 1489
 Kravtsov A. V., Vikhlinin A., Nagai D., 2006, *ApJ*, 650, 128
 Landry D., Bonamente M., Giles P., Maughan B., Joy M., Murray S., 2013, *MNRAS*, 433, 2790
 Limousin M., Morandi A., Sereno M., Meneghetti M., Ettori S., Bartelmann M., Verdugo T., 2013, *Space Science Reviews*, 177, 155
 Mahdavi A., Hoekstra H., Babul A., Bildfell C., Jeltrema T., Henry J. P., 2013, *ApJ*, 767, 116
 Mantz A., Allen S. W., Rapetti D., Ebeling H., 2010, *MNRAS*, 406, 1759
 Marrone D. P. et al., 2012, *ApJ*, 754, 119
 Maughan B. J., Giles P. A., Randall S. W., Jones C., Forman W. R., 2012, *MNRAS*, 421, 1583
 Meneghetti M., Fedeli C., Zitrin A., Bartelmann M., Broadhurst T., Gottlöber S., Moscardini L., Yepes G., 2011, *A&A*, 530, A17
 Meneghetti M., Rasia E., Merten J., Bellagamba F., Ettori S., Maz-zotta P., Dolag K., Marri S., 2010, *A&A*, 514, A93
 Nelson K., Lau E. T., Nagai D., Rudd D. H., Yu L., 2014, *ApJ*, 782, 107
 Oguri M., Blandford R. D., 2009, *MNRAS*, 392, 930
 Okabe N., Smith G. P., Umetsu K., Takada M., Futamase T., 2013, *arXiv*: 1302.2728
 Okabe N., Takada M., Umetsu K., Futamase T., Smith G. P., 2010, *PASJ*, 62, 811
 Planck Collaboration et al., 2013a, *ArXiv*: 1303.5089
 Planck Collaboration et al., 2013b, *ArXiv*: 1303.5076
 Planck Collaboration et al., 2013c, *ArXiv*: 1303.5080
 Planck Collaboration et al., 2013d, *A&A*, 550, A129
 Rasia E. et al., 2012, *New Journal of Physics*, 14, 055018
 Rines K., Diaferio A., 2006, *AJ*, 132, 1275
 Roncarelli M., Ettori S., Borgani S., Dolag K., Fabjan D., Moscardini L., 2013, *MNRAS*, 432, 3030
 Rozo E., Bartlett J. G., Evrard A. E., Rykoff E. S., 2014a, *MNRAS*, 438, 78
 Rozo E., Evrard A. E., Rykoff E. S., Bartlett J. G., 2014b, *MNRAS*, 438, 62
 Rozo E., Rykoff E. S., Bartlett J. G., Evrard A., 2014c, *MNRAS*, 438, 49

- Rozo E. et al., 2010, *ApJ*, 708, 645
 Sereno M., 2014, in preparation
 Sereno M., Etti S., 2014, *MNRAS*, submitted
 Sereno M., Etti S., Umetsu K., Baldi A., 2013, *MNRAS*, 428, 2241
 Sereno M., Umetsu K., 2011, *MNRAS*, 416, 3187
 Sereno M., Zitri A., 2012, *MNRAS*, 419, 3280
 Umetsu K., Broadhurst T., Zitri A., Medezinski E., Coe D., Postman M., 2011, *ApJ*, 738, 41
 Umetsu K. et al., 2014, *ArXiv*: 1404.1375
 Vikhlinin A. et al., 2009, *ApJ*, 692, 1033
 Voit G. M., 2005, *Reviews of Modern Physics*, 77, 207
 von der Linden A. et al., 2014, *ArXiv*:1402.2670